Memo version 1.0

BESIII Analysis Memo

DocDB-???

BAM-???

September 21, 2022

Observation of $\psi(3686) \to \Lambda\bar{\Lambda}\eta'$

Tingjun Jiang[a], Shuangshi Fang[b], and Qingjun Xu[a]

[a]*Hangzhou Normal University*
[b]*Institute of High Energy Physics*

Internal Referee Committee

Ref1 xx (Chair)[d], Ref2 xx[e], and Ref3 xx[f]

[d]*xxx*
[e]*xxx*
[f]*xxx*

DocDB : http://docbes3.ihep.ac.cn/cgi-bin/DocDB/ShowDocument?docid=???

Hypernews : http://hnbes3.ihep.ac.cn/HyperNews/get/paper???.html

Abstract

Based on the 2.7 billion of $\psi(3686)$ events collected with the BESIII detector , the $\psi(3686) \to \Lambda\bar{\Lambda}\eta'$ is observed for the first time. With the two decay modes of $\eta' \to \gamma\pi^+\pi^-$ and $\eta' \to \eta\pi^+\pi^-$, the statistical significances of $\psi(3686) \to \Lambda\bar{\Lambda}\eta'$ are found to be 6.8σ and 10σ, respectively. With these two η' decays, the branching fractions of $\psi(3686) \to \Lambda\bar{\Lambda}\eta'$ are measured to be $(6.97 \pm 1.13 \pm 0.82) \times 10^{-6}$ and$(8.22 \pm 1.12 \pm 0.87) \times 10^{-6}$, where the first uncertainties are statistical and the second systematic. And the average branching fraction of $\psi(3686) \to \Lambda\bar{\Lambda}\eta'$ is measured to be $(7.58 \pm 1.10) \times 10^{-6}$, where the uncertainty includes both statistical and systematic.

Contents

1 Introduction

Being the bound state of a c and an anti-c quarks, a charmonium state is related to long-range (i.e. confinement) interactions, which provide information on non-perturbative QCD in the low energy region, where the heavy quark effective theory is not well applicable. Therefore, the study of charmonium mesons is of particular interest since they are a bridge between the light and heavy quarks, which will provide knowledge of its structure and may shed light on perturbative and non-perturbative strong interactions in this energy region. The high production rate of baryons in charmonium decays, combined with the large data samples of J/ψ and $\psi(3686)$ decays produced from e^+e^- annihilations, provides an excellent opportunity for studying excited baryons.

The decays of $J/\psi(\psi(3686)) \to \Lambda\bar{\Lambda}\pi^0(\eta)$ were studied [1, 2], which have studied 12% rule. But the experimental study of $J/\psi(\psi(3686)) \to \Lambda\bar{\Lambda}\eta'$ has never been done yet. Due to the limited phase space, it is hard to search for $J/\psi \to \Lambda\bar{\Lambda}\eta'$. At present, a sample of 2.7 billion $\psi(3686)$ events produced in e^+e^- annihilation [3] is available at the BESIII experimental, which allows to have a study on the decays of $\psi(3686) \to \Lambda\bar{\Lambda}\eta'$, and provides an opportunity to search for $\Lambda^*(\bar{\Lambda}^*)$, which consists of $\Lambda\eta'(\bar{\Lambda}\eta')$.

2 BEPCII and BESIII Detector

BEPCII is a double-ring e^+e^- collider that has reached the peak luminosity of 10^{33} cm^2 s^{-1} at the center-of-mass (CM) energy of 3.773 GeV. The cylindrical core of the BESIII detector consists of a helium-based main drift chamber (MDC), a plastic scintillator time-of-flight (TOF) system, and a CsI(Tl) electromagnetic calorimeter (EMC), which are all enclosed in a super conducting solenoidal magnet with a field strength of 1.0 T for the $\psi(3686)$ data. The solenoid is supported by an octagonal flux-return yoke with resistive plate counter modules interleaved with steel as muon identifier. The acceptance for charged particles and photons is 93% of the 4π stereo angle, and the charged-particle momentum resolution at 1 GeV/c is 0.5%. The photon energy resolution is 2.5% (5%) at 1.0 GeV in the barrel region (end-caps regions). More details about the experimental apparatus can be found in Ref. [4] .

Simulated data samples produced with a GEANT4-based Monte Carlo (MC) package [6], which includes the geometric description of the BESIII detector and the detector response, are used to determine detection efficiencies and to estimate backgrounds. The simulation models the beam energy spread and initial state radiation (**ISR**) in the e^+e^- annihilations with the generator KKMC [7, 8]. The inclusive MC sample includes the production of the $\psi(3686)$ resonance, the known decay modes are modelled with EVTGEN [9, 10] using branching fractions taken from the Particle Data Group [3], and the remaining unknown charmonium decays are modelled with LUNDCHARM [11].

3 Datasets

The analysis is based on a sample of 2.7×10^9 $\psi(3686)$ events [12, 13], collected with the BESIII detector operating at the BEPCII collider , and the software framework used for the data analysis is BESIII Offline Software System (Boss). The uesed BOSS version in this study is 709. About 2.7 billion $\psi(3686)$ inclusive MC sample is used to investigate possible background. And an exclusive MC samples of 2.6×10^6 $\psi(3686)$ events is generated to optimize the selection criteria and determine the corresponding selection efficiencies. The data samples taken at center-of-mass energy of 3.65GeV/c^2 and 3.682GeV/c^2 with integrated luminosities of 410 pb^{-1} and 404 pb^{-1} [14] , used to analysis continuum processes . Table.1 shows the decay card we use to generate the decay channel of $\psi(3686) \to \Lambda\bar{\Lambda}\eta'$, $\eta' \to \gamma\pi^+\pi^-/\eta' \to \eta\pi^+\pi^-$.

Table 1: Exclusive MC samples

Decay Mode	Generator	Number of events
$\psi(3686) \to \Lambda\bar{\Lambda}\eta', \eta' \to \gamma\pi^+\pi^-$	$PHSP, DIY\_Etap2gpipi\_box0$	2.6×10^6
$\psi(3686) \to \Lambda\bar{\Lambda}\eta', \eta' \to \eta\pi^+\pi^-, \eta \to \gamma\gamma$	$PHSP, DIY\_pipieta$	2.6×10^6

4 Event selection

In this analysis, the $\Lambda(\bar{\Lambda})$ is reconstructed in $\Lambda \to p\pi^-(\bar{p}\pi^+)$, while the η' are detected with its two decay modes of $\eta' \to \gamma\pi^+\pi^-$ (**Mode I**) and $\eta' \to \eta\pi^+\pi^-, \eta \to \gamma\gamma$ (**Mode II**).

The possible final states for $\psi(3686) \to \Lambda\bar{\Lambda}\eta'$ are then $p\bar{p}\pi^+\pi^-\pi^+\pi^-\gamma$ and $p\bar{p}\pi^+\pi^-\pi^+\pi^-\gamma\gamma$. The following common selection criteria, including charged track selection, particle identification and Λ reconstruction, are used to select candidate events.

• **Charged Tracks**: The polar angle in the MDC must satisfy $|cos\theta|< 0.93$, the points of closest approach to the interaction point(IP) is no requirement for $p(\bar{p})$ and $\pi^-(\pi^+)$ decays from $\Lambda(\bar{\Lambda})$. For charged tracks , the final states of two processes are both $p\bar{p}\pi^+\pi^+\pi^-\pi^-$, the number of charged tracks requires more than 6.

• **PID**: For each charged track, both TOF and dE/dx information are combined to form Particle IDentification (PID) confidence levels for the π, K, and p hypotheses (Prob(i), i = π, K, p). A charged track is identified as a pion or proton if its Prob is larger than those for any other assignment.

• $\Lambda\bar{\Lambda}$ **Reconstruction**: The Λ and $\bar{\Lambda}$ candidates are reconstructed by combining pairs of oppositely charged tracks with pion and proton mass hypotheses, fulfilling a secondary vertex constraint [15] . No requirement to χ^2 of second vertex fit or decay length of $\Lambda(\bar{\Lambda})$. Events with at least one $p\pi^-(\Lambda)$ and one $\bar{p}\pi^+(\bar{\Lambda})$ candidate are selected. In the case of multiple $\Lambda\bar{\Lambda}$ pair candidates, one pair of $\Lambda\bar{\Lambda}$ with minimal value of $(M_{p\pi^-} - M_\Lambda)^2 + (M_{\bar{p}\pi^+} - M_{\bar{\Lambda}})^2$ is chosen.

• $\pi^+\pi^-$ **Reconstruction**: For π not used in $\Lambda\bar{\Lambda}$ reconstruction, the distance of closest approach to the interaction point (IP) must be less than 10 cm in the beam direction and less than 1 cm in the perpendicular direction. Looping all over the $\pi^+\pi^-$ combinations to pass a vertex fit, one pair of $\pi^+\pi^-$ with minimal χ^2 of vertex fit kept.

• **Good Photon Selection**: Photon candidates, reconstructed by clustering EMC crystal energies, must have a minimum energy of 25 MeV for the barrel ($|cos\theta|< 0.80$) and 50 MeV for the end- cap ($0.86 < |cos\theta|< 0.92$), must satisfy EMC cluster timing requirement of $[0, 700]$ ns to suppress electronic noise and energy deposits unrelated to the event, and be separated by at least 10° from the nearest charged track to exclude energy deposits from charged particles. At least one photon candidates is required for the **Mode I**, while at least two photon candidates for **Mode II**.

• **Kinematic fit**: The selected events are fitted kinematically. The kinematic fit adjusts the track energy and momentum within the measured errors so as to satisfy energy and momentum conservation for the given event hypothesis. This improves resolution, selects the correct charged-particle assignment for the tracks, and reduces background. When the number of photons in an event exceeds the minimum, all combinations are tried, and the combination with the smallest χ^2 is retained.

5 Analysis of $\psi(3686) \to \Lambda\bar{\Lambda}\eta', \eta' \to \gamma\pi^+\pi^-$

5.1 Final events selection

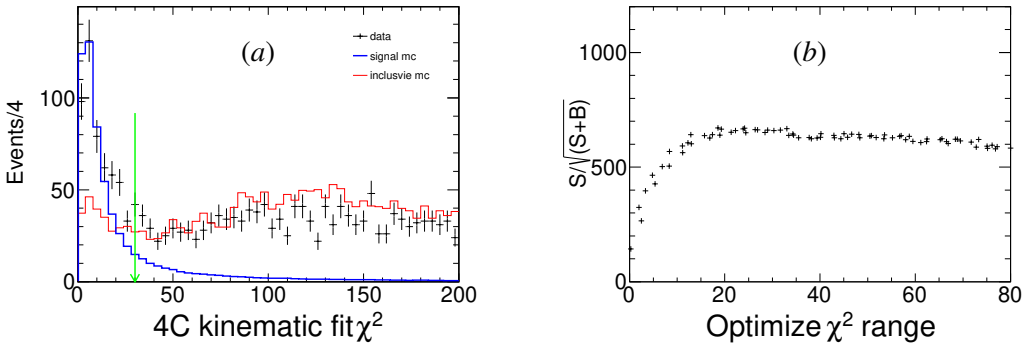

Figure 1: The distribution 4C kinematic fit χ^2 (a) and the optimization result (b).

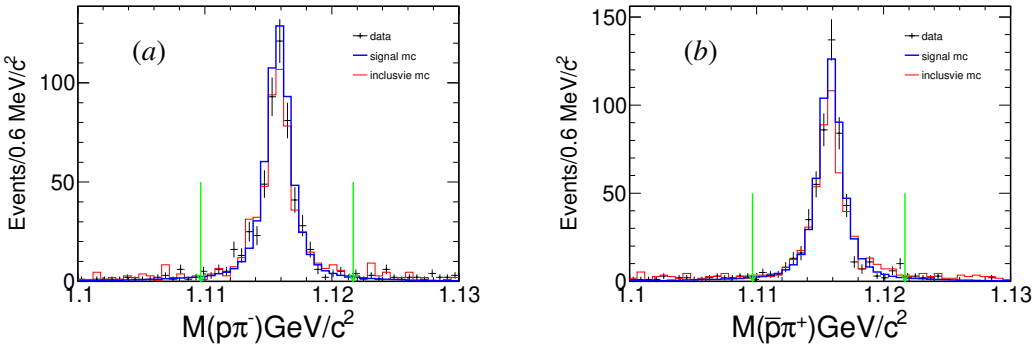

Figure 2: The invariant mass distributions of $p\pi^-$ (a) and $\bar{p}\pi^+$ (b).

The χ^2_{4C} of the kinematic fit is required to be less than 30 from an optimization ($S/\sqrt{S+B}$) as illustrated in Fig.1(b), where "S" represent the signal and "$S+B$" is data sample. Figure 2 shows the $p\pi^-$ and $\bar{p}\pi^+$ invariant mass distributions, respectively, and the clear peak at the Λ and $\bar{\Lambda}$ mass are clearly observed. We then require that the invariant mass distribution of $p\pi^-(\bar{p}\pi^+)$ satisfies $|M_{p\pi^-(\bar{p}\pi^+)} - M_{\Lambda(\bar{\Lambda})}| < 6$ MeV/c^2 , which are saved as $\Lambda(\bar{\Lambda})$ candidates.

To remove the background events from $\psi(3686) \to \Sigma^0\bar{\Lambda}\pi^+\pi^- + c.c$, the invariant mass of $\gamma\Lambda(\gamma\bar{\Lambda})$, as displayed in Fig.3, is required not to be in the mass region of $\Sigma^0(\bar{\Sigma^0})$, $|M_{\gamma\Lambda(\bar{\Lambda})} - M_{\Sigma^0(\bar{\Sigma}^0)}| > 10$ MeV/c^2.

Figure 4 shows the invariant mass recoiling against the $\pi^+\pi^-$, where J/ψ peak, coming from $J/\psi \to \gamma\Lambda\bar{\Lambda}$, is clear. We then require $|M^{\pi^+\pi^-}_{recoil} - M_{J/\psi}| > 8$ MeV/c^2 to suppress the background events from $\psi(3686) \to \pi^+\pi^- J/\psi, J/\psi \to \gamma\Lambda\bar{\Lambda}$.

We reject events within χ_{cJ} mass region (Fig.5) as $|M^{\gamma}_{recoil} - M_{\chi_{c0}}| < 16$ MeV/c^2, $|M^{\gamma}_{recoil} - M_{\chi_{c1}}| <$

10MeV/c^2 and $|M^{\gamma}_{recoil} - M_{\chi_{c2}}| < 10$ MeV/c^2 to reduce the backgrounds from $\psi(3686) \to \gamma\chi_{cJ}(J = 0, 1, 2)$, $\chi_{cJ} \to \Lambda\bar{\Lambda}\pi^+\pi^-$. Figure 6 shows the scatter plots of $\Lambda\pi^-$ versus $\bar{\Lambda}\pi^+$ and $\bar{\Lambda}\pi^-$ versus $\Lambda\pi^+$ respectively. The green boxes indicate the cuts to remove backgrounds contributed from $\psi(3686) \to \Xi^-\bar{\Xi}^+$ and $\psi(3686) \to \Sigma^{*-}\bar{\Lambda}\pi^+ + c.c.$

After the above requirements, the invariant mass of $\gamma\pi^+\pi^-$ is shown in Fig.7, where the η' peak is clearly observed. The Cuts Flow for each selection criteria is summarized in Table2. And the detection efficiency is determined to be 6.54%, which is obtained from a MC sample of 2.6×10^6 $\psi(3686) \to \Lambda\bar{\Lambda}\eta'$ phase space events.

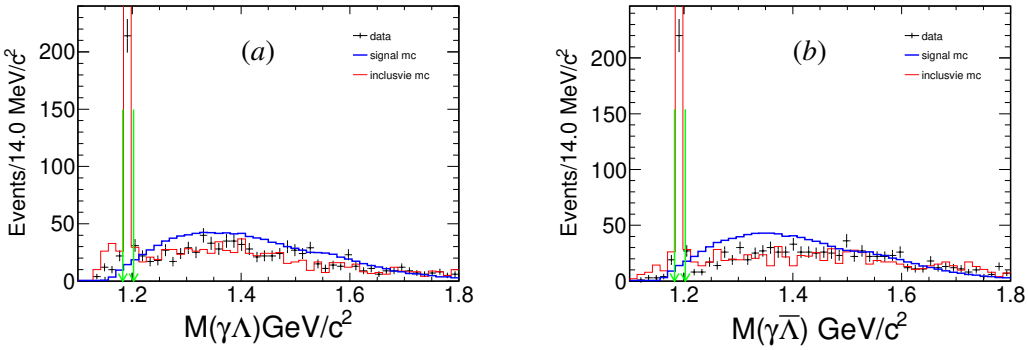

Figure 3: The mass distribution of $\gamma\Lambda$ and $\gamma\bar{\Lambda}$.

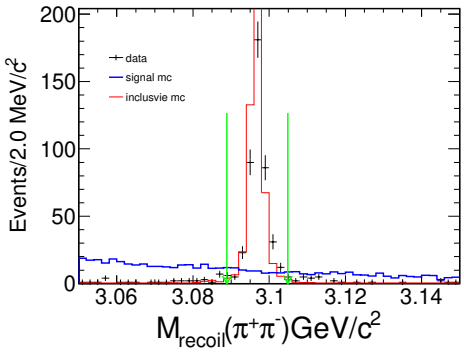

Figure 4: The invariant mass recoiling against the $\pi^+\pi^-$.

5.2 Background analysis

To investigate the possible background contributions, the same selection criteria are applied to an inclusive MC sample of 2.7 billion events of $\psi(3686)$ inclusive decays. A topological analysis of the surviving events is performed with the generic tool TopoAna [16]. Topological result is shown in Table.3. The results indicate that the background events mainly have an approximately flat distribution.

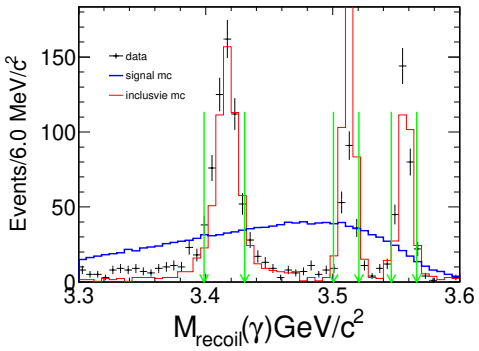

Figure 5: The distribution of invariant mass recoiling against the radiative photon.

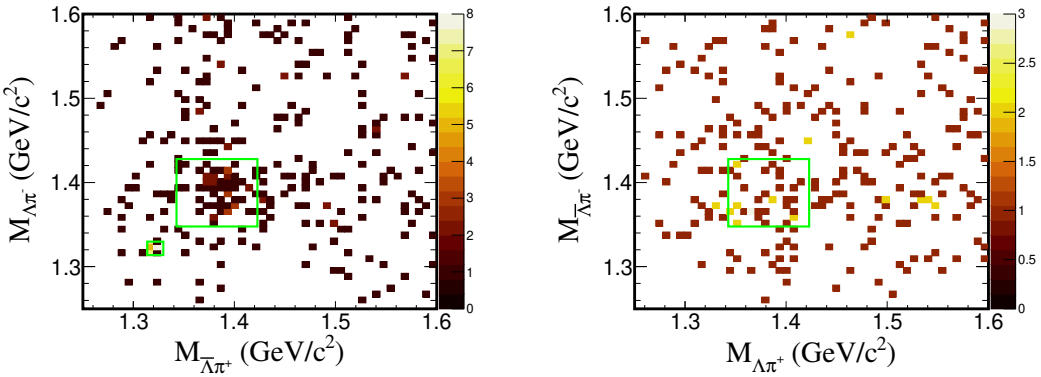

(*a*) (*b*)

Figure 6: The scatter plots of $\Lambda\pi^-$ versus $\bar{\Lambda}\pi^+$ (a) and $\bar{\Lambda}\pi^-$ versus $\Lambda\pi^+$ (b). The small box shown in (a) is the scatter plots of Ξ^- versus $\bar{\Xi}^+$, and the mass window determined to be 8 MeV/c^2. And the mass window of the two big boxes which indicated Σ^{*-} versus $\bar{\Sigma}^{*+}$(+ c.c) are 40 MeV/c^2.

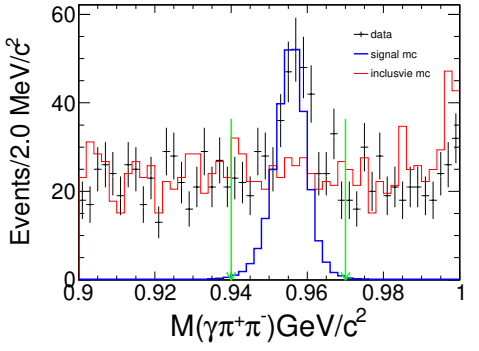

Figure 7: The invariant mass distribution of $\gamma\pi^+\pi^-$

Table 2: Cut flow

Criteria	Efficiency(%)
$N_{charged} \geqslant 6$	42.59
Pass PID	30.01
$\Lambda\bar{\Lambda}$ reconstruction	29.06
$\pi^+\pi^-$ vertex fit	23.57
$N_\gamma \geqslant 1$	23.44
Pass 4C	15.14
$\chi^2_{4C} < 30$	10.35
$\lvert M_{p\pi^-(\bar{p}\pi^+)} - M_{\Lambda(\bar{\Lambda})}\rvert < 6$ MeV/c^2	9.23
$\lvert M_{\gamma\Lambda(\bar{\Lambda})} - M_{\Sigma^0(\bar{\Sigma}^0)}\rvert > 10$ MeV/c^2	8.81
$\lvert M^{\pi^+\pi^-}_{recoil} - M_{J/\psi}\rvert > 8$ MeV/c^2	8.77
veto χ_{cJ} mass region	6.83
veto $\Sigma(1385)$ and $\Xi^-(\bar{\Xi}^+)$ mass region	6.54

Table 3: The dominant background contributions to $\psi(3686) \to \Lambda\bar{\Lambda}\eta', \eta' \to \gamma\pi^+\pi^-$.

No.	Decay tree	iDcyTr	Number of events
1	$\psi(3686) \to \pi^+\pi^- J/\psi, J/\psi \to \Lambda\bar{\Lambda}\gamma, \Lambda \to \pi^- p, \bar{\Lambda} \to \pi^+\bar{p}$	1	159
2	$\psi(3686) \to \chi_{c0}\gamma, \chi_{c0} \to \pi^+\Lambda\bar{\Sigma}^{*-}, \Lambda \to \pi^- p, \bar{\Sigma}^{*-} \to \pi^-\bar{\Lambda}, \bar{\Lambda} \to \pi^+\bar{p}$	0	38
3	$\psi(3686) \to \chi_{c0}\gamma, \chi_{c0} \to \pi^+\Sigma^{*-}\bar{\Lambda}, \Sigma^{*-} \to \pi^-\Lambda, \bar{\Lambda} \to \pi^+\bar{p}, \Lambda \to \pi^- p$	3	29
4	$\psi(3686) \to \chi_{c0}\gamma, \chi_{c0} \to \pi^-\bar{\Lambda}\Sigma^{*+}, \bar{\Lambda} \to \pi^+\bar{p}, \Sigma^{*+} \to \pi^+\Lambda, \Lambda \to \pi^- p$	10	29
5	$\psi(3686) \to \chi_{c0}\gamma, \chi_{c0} \to \pi^-\bar{\Sigma}^{*+}\Lambda, \bar{\Sigma}^{*+} \to \pi^+\bar{\Lambda}, \Lambda \to \pi^- p, \bar{\Lambda} \to \pi^+\bar{p}$	14	29
6	$\psi(3686) \to \chi_{c2}\gamma, \chi_{c2} \to \pi^-\bar{\Lambda}\Sigma^{*+}, \bar{\Lambda} \to \pi^+\bar{p}, \Sigma^{*+} \to \pi^+\Lambda, \Lambda \to \pi^- p$	36	13
7	$\psi(3686) \to \chi_{c0}\gamma, \chi_{c0} \to K^{*+}\bar{p}\Lambda, K^{*+} \to \pi^+ K^0, \Lambda \to \pi^- p, K^0 \to K^0_S,$ $K^0_S \to \pi^+\pi^-$	48	13
8	$\psi(3686) \to \chi_{c2}\gamma, \chi_{c2} \to \pi^-\bar{\Sigma}^{*+}\Lambda, \bar{\Sigma}^{*+} \to \pi^+\bar{\Lambda}, \Lambda \to \pi^- p, \bar{\Lambda} \to \pi^+\bar{p}$	25	10
9	$\psi(3686) \to \chi_{c0}\gamma, \chi_{c0} \to K^{*-} p\bar{\Lambda}, K^{*-} \to \pi^-\bar{K}^0, \bar{\Lambda} \to \pi^+\bar{p}, \bar{K}^0 \to K^0_S,$ $K^0_S \to \pi^+\pi^-$	39	10
10	$\psi(3686) \to \chi_{c1}\gamma, \chi_{c1} \to \pi^-\bar{\Lambda}\Sigma^{*+}, \bar{\Lambda} \to \pi^+\bar{p}, \Sigma^{*+} \to \pi^+\Lambda, \Lambda \to \pi^- p$	26	10
11	$\psi(3686) \to \pi^-\bar{\Sigma}^{*+}\Lambda\gamma^f, \bar{\Sigma}^{*+} \to \pi^+\bar{\Lambda}, \Lambda \to \pi^- p, \bar{\Lambda} \to \pi^+\bar{p}$	50	10
12	$\psi(3686) \to \chi_{c2}\gamma, \chi_{c2} \to \pi^+\Lambda\bar{\Sigma}^{*-}, \Lambda \to \pi^- p, \bar{\Sigma}^{*-} \to \pi^-\bar{\Lambda}, \bar{\Lambda} \to \pi^+\bar{p}$	7	9
13	$\psi(3686) \to \chi_{c1}\gamma, \chi_{c1} \to \pi^+\Lambda\bar{\Sigma}^{*-}, \Lambda \to \pi^- p, \bar{\Sigma}^{*-} \to \pi^-\bar{\Lambda}, \bar{\Lambda} \to \pi^+\bar{p}$	11	8
14	$\psi(3686) \to \chi_{c1}\gamma, \chi_{c1} \to \pi^-\bar{\Sigma}^{*+}\Lambda, \bar{\Sigma}^{*+} \to \pi^+\bar{\Lambda}, \Lambda \to \pi^- p, \bar{\Lambda} \to \pi^+\bar{p}$	13	8
15	$\psi(3686) \to \chi_{c2}\gamma, \chi_{c2} \to \rho^0\Lambda\bar{\Lambda}, \rho^0 \to \pi^+\pi^-, \Lambda \to \pi^- p, \bar{\Lambda} \to \pi^+\bar{p}$	27	7
16	$\psi(3686) \to \pi^+\Lambda\bar{\Sigma}^{*-}\gamma^f, \Lambda \to \pi^- p, \bar{\Sigma}^{*-} \to \pi^-\bar{\Lambda}, \bar{\Lambda} \to \pi^+\bar{p}$	35	7
17	$\psi(3686) \to \pi^-\bar{\Lambda}\Sigma^{*+}, \bar{\Lambda} \to \pi^+\bar{p}, \Sigma^{*+} \to \pi^+\Lambda, \Lambda \to \pi^- p$	21	6
18	$\psi(3686) \to \eta'\Delta^{++}\bar{\Delta}^{--}, \eta' \to \pi^+\pi^-\gamma^F, \Delta^{++} \to \pi^+ p, \bar{\Delta}^{--} \to \pi^-\bar{p}$	43	1
others	Including 91 decay channels		175

To estimate the number of background events coming directly from the e^+e^- annihilation, the same analysis is performed on data samples taken at center-of-mass energy of 3.65 GeV and 3.682 GeV, respectively, corresponding to the integrated luminosities of 410 pb^{-1} and 404 pb^{-1}. The $\gamma\pi^+\pi^-$ invariant mass distributions are shown in Fig.8, where no evident η' is seen. Hence we ignored the background contribution from this source.

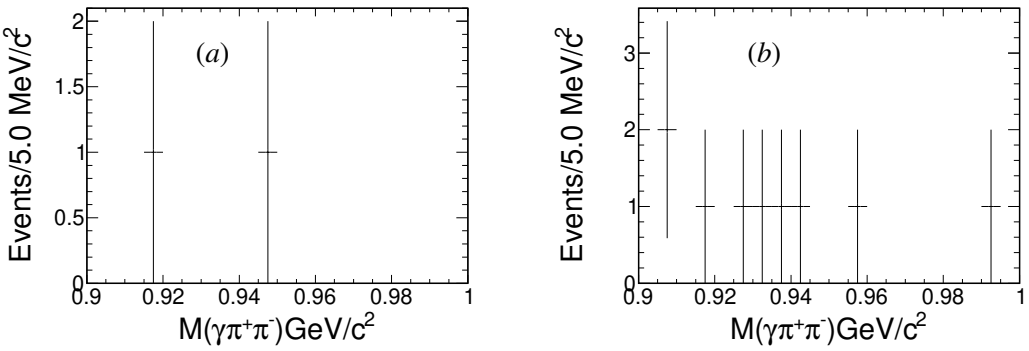

Figure 8: Invariant mass distributions of $\gamma\pi^+\pi^-$ at center-of-mass energy of 3.65 GeV/c^2 (a) and 3.682 GeV/c^2 (b).

6 Analysis of $\eta' \to \eta\pi^+\pi^-$

6.1 Final events selection

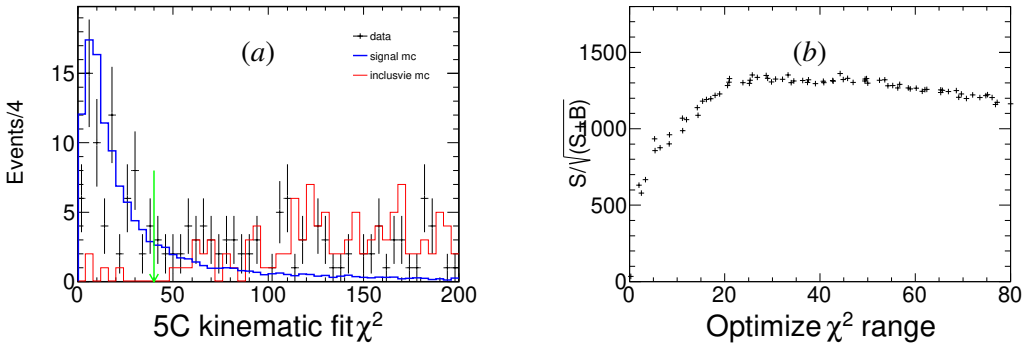

Figure 9: The distribution of 5C kinematic fit χ^2 (a) and the optimization result (b).

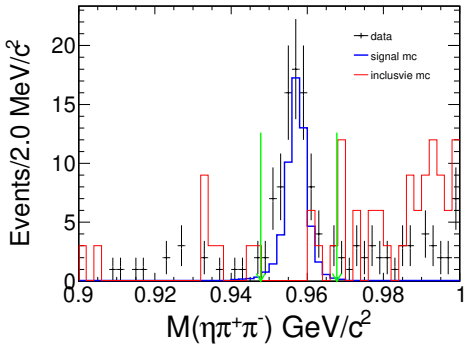

Figure 10: The invariant mass distribution of $\eta\pi^+\pi^-$

In case of $\psi(3686) \to \Lambda\bar{\Lambda}\eta', \eta' \to \eta\pi^+\pi^-$, a five-constraint (5C) kinematic fit is performed for each $\Lambda\bar{\Lambda}\pi^+\pi^-\gamma\gamma$ combination. The fit enforces energy-momentum conservation and constrains the invariant masses of the photon pair to the nominal η mass. The 5C kinematic fit χ^2 (Fig. 9(a)) is required to be less than 40 in accordance with the optimization illustrated in Fig. 9 (b). A mass requirement of $M_{p\pi^-(\bar{p}\pi^+)} \in (1.108, 1.123)$ GeV/c^2 is applied to select $\Lambda/\bar{\Lambda}$ candidates as shown in Fig.11. The background events from $\psi(3686) \to \eta J/\psi, J/\psi \to \Lambda\bar{\Lambda}\pi^+\pi^-$, as displayed in Fig.12 , are rejected by requiring $|M^{\eta}_{recoil} - M_{J/\psi}|> 10$ MeV/c^2, where M^{η}_{recoil} is the invariant mass recoiling against η.

With a sample of MC events generated with the uniform phase space, the detection efficiency is determined to be 4.58%. And the impacts for each selection criteria are presented in Table.4.

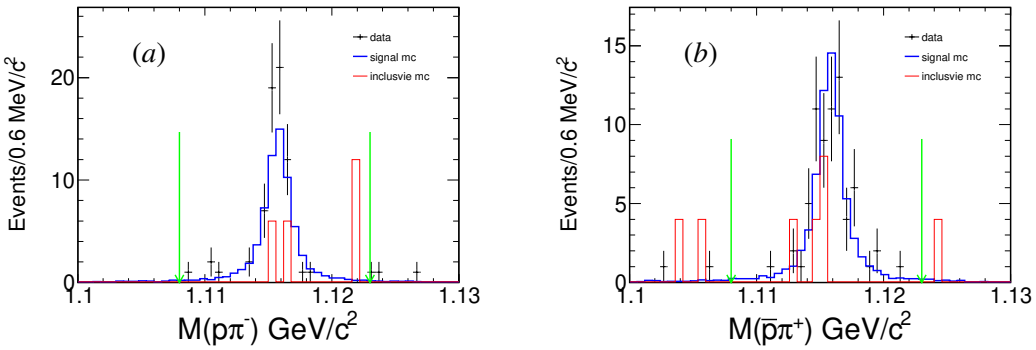

Figure 11: The invariant mass distribution of $p\pi^-$ (a) and $\bar{p}\pi^+$ (b)

.

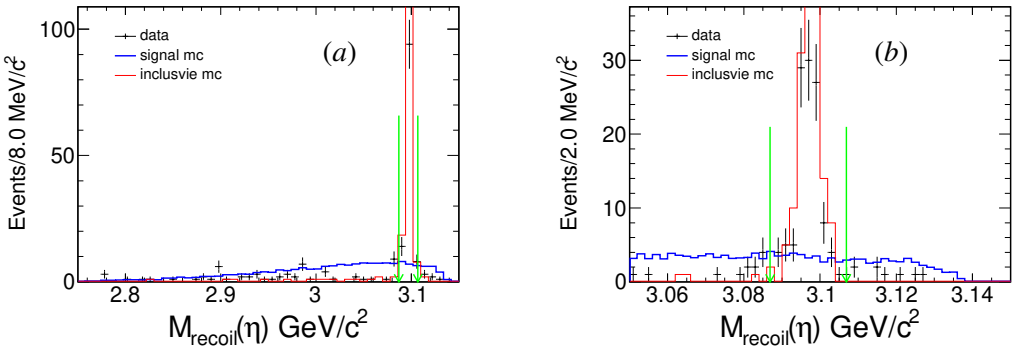

Figure 12: The distribution of invariant mass recoiling against η (a) and the distribution in region (3.05,3.15) GeV/c^2 (b).

Table 4: Cut flow

Criteria	Efficiency(%)
$N_{charged} \geqslant 6$	36.05
Pass PID	23.93
$\Lambda\bar{\Lambda}$ reconstruction	23.11
$\pi^+\pi^-$ vertex fit	15.86
$N_\gamma \geqslant 2$	15.41
Pass 5C	8.24
$\chi^2_{5C} < 40$	5.56
$M_{p\pi^-(\bar{p}\pi^+)} \in (1.108, 1.123)$ GeV/c^2	5.09
$\lvert M^{\eta}_{recoil} - M_{J/\psi}\rvert > 10$ MeV/c^2	4.58

Table 5: The dominant background contributions to $\psi(3686) \to \Lambda\bar{\Lambda}\eta', \eta' \to \eta\pi^+\pi^-$.

No.	Decay tree	iDcyTr	number of events
1	$\psi(3686) \to \pi^+\pi^- J/\psi, J/\psi \to \eta\Lambda\bar{\Lambda}, \eta \to \gamma\gamma, \Lambda \to \pi^- p, \bar{\Lambda} \to \pi^+\bar{p}$	7	8
2	$\psi(3686) \to \eta J/\psi, \eta \to \pi^0\pi^+\pi^-, J/\psi \to \Lambda\bar{\Lambda}\gamma, \Lambda \to \pi^- p, \bar{\Lambda} \to \pi^+\bar{p}$	6	5
3	$\psi(3686) \to \chi_{c1}\gamma, \chi_{c1} \to J/\psi\gamma, J/\psi \to \pi^+\pi^-\Lambda\bar{\Lambda}, \Lambda \to \pi^- p, \bar{\Lambda} \to \pi^+\bar{p}$	1	4
4	$\psi(3686) \to \eta\Sigma^{*+}\bar{\Sigma}^{*-}, \eta \to \gamma\gamma, \Sigma^{*+} \to \pi^+\Lambda, \bar{\Sigma}^{*-} \to \pi^-\bar{\Lambda}, \Lambda \to \pi^- p,$ $\bar{\Lambda} \to \pi^+\bar{p}$	2	4
5	$\psi(3686) \to \chi_{c0}\gamma, \chi_{c0} \to \pi^0\Sigma^{*+}\bar{\Sigma}^{*-}, \Sigma^{*+} \to \pi^+\Lambda, \bar{\Sigma}^{*-} \to \pi^-\bar{\Lambda}, \Lambda \to \pi^- p,$ $\bar{\Lambda} \to \pi^+\bar{p}$	12	4
6	$\psi(3686) \to \eta\bar{\Sigma}^{*+}\Sigma^{*-}, \eta \to \gamma\gamma, \bar{\Sigma}^{*+} \to \pi^+\bar{\Lambda}, \Sigma^{*-} \to \pi^-\Lambda, \bar{\Lambda} \to \pi^+\bar{p},$ $\Lambda \to \pi^- p$	14	4
7	$\psi(3686) \to \pi^0\pi^0 J/\psi, J/\psi \to \pi^+\pi^-\Lambda\bar{\Lambda}, \Lambda \to \pi^- p, \bar{\Lambda} \to \pi^+\bar{p}$	4	3
others	Including 11 decay channels		14

6.2 Background analysis

To ensure that the η' peak is not from background events, a study was performed with a inclusive MC sample of 2.7 billion $\psi(3686)$ events and the dominant possible background contributions are shown in Table.5. The results indicate that none of these background sources produce a peak in the $\pi^+\pi^-\eta$ invariant mass spectrum near the η' mass.

The two data samples taken at center-of-mass energy of 3.65 GeV and 3.682 GeV, respectively, corresponding to the integrated luminosities of 410 pb^{-1} and 404 pb^{-1}, are also used to investigate the background contributions directly from e^+e^- annihilations. With the same analysis, it is found that only 1 event is selected from the data taken at center-of-mass energy of 3.682 GeV, as shown in Fig. 13, while no event remains in mass region of [0.9, 1.0] GeV/c^2 for the data taken center-of-mass energy of 3.65 GeV. Therefore, we ignored the background contribution from this source.

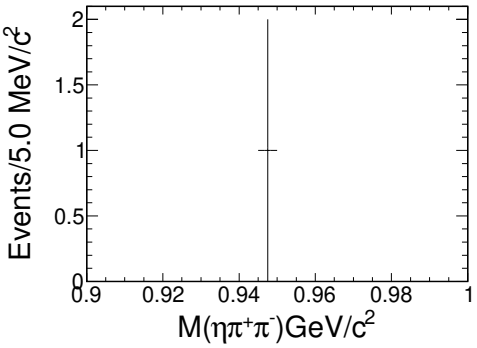

Figure 13: Invariant mass distribution of $\eta\pi^+\pi^-$ at center-of-mass energy of and 3.682 GeV/c^2 .

7 Branching fraction measurement

The $\psi(3686) \to \Lambda\bar{\Lambda}\eta'$ signal yield is obtained from an extended unbinned maximum likelihood fit to the $\gamma\pi^+\pi^-(\eta\pi^+\pi^-)$ invariant mass distribution. The total probability density function consists of a signal and no-peaking background contribution. The signal component is modeled with the MC simulated signal shape convolved with a Gaussian function to account for a possible difference in the mass resolution between data and MC simulation, the non-peaking background is parameterized by a second order Chebychev function.

The fits shown in Figure.14 yield 148 ± 24 and 70 ± 10 $\psi(3686) \to \Lambda\bar{\Lambda}\eta'$ events respectively. With the detection efficiencies, 6.5% for **Mode I** and 4.58% for **Mode II**, the branching fractions are calculated to be

$$\begin{aligned}\mathcal{B}(\psi(3686) \to \Lambda\bar{\Lambda}\eta', \eta' \to \gamma\pi^+\pi^-) &= \frac{N^{obs}_{\gamma\pi\pi}}{N_{\psi(3686)} \times \mathcal{B}(\Lambda \to p\pi^-) \times \mathcal{B}(\bar{\Lambda} \to \bar{p}\pi^+) \times \mathcal{B}(\eta' \to \gamma\pi^+\pi^-) \times \epsilon_1} \\ &= (6.97 \pm 1.13) \times 10^{-6}\end{aligned} \tag{1}$$

and

$$\begin{aligned}&\mathcal{B}(\psi(3686) \to \Lambda\bar{\Lambda}\eta', \eta' \to \eta\pi^+\pi^-) \\ &= \frac{N^{obs}_{\eta\pi\pi}}{N_{\psi(3686)} \times \mathcal{B}(\Lambda \to p\pi^-) \times \mathcal{B}(\bar{\Lambda} \to \bar{p}\pi^+) \times \mathcal{B}(\eta' \to \eta\pi^+\pi^-) \times \mathcal{B}(\eta \to \gamma\gamma) \times \epsilon_2} \\ &= (8.22 \pm 1.12) \times 10^{-6},\end{aligned} \tag{2}$$

where $N^{obs}_{\gamma\pi\pi}$ and $N^{obs}_{\eta\pi\pi}$ are the observed number of signal candidates; $N_{\psi(3686)} = 2.7 \times 10^9$ is the number of $\psi(3686)$ events; ϵ_1 and ϵ_2 are the detection efficiency obtained from MC simulation respectively; $\mathcal{B}(\Lambda \to p\pi^-)$, $\mathcal{B}(\bar{\Lambda} \to \bar{p}\pi^+)$, $\mathcal{B}(\eta' \to \gamma\pi^+\pi^-)$, $\mathcal{B}(\eta' \to \eta\pi^+\pi^-)$ and $\mathcal{B}(\eta \to \gamma\gamma)$ are the corresponding branching fractions from PDG [3]. Here the uncertainties are statistical only.

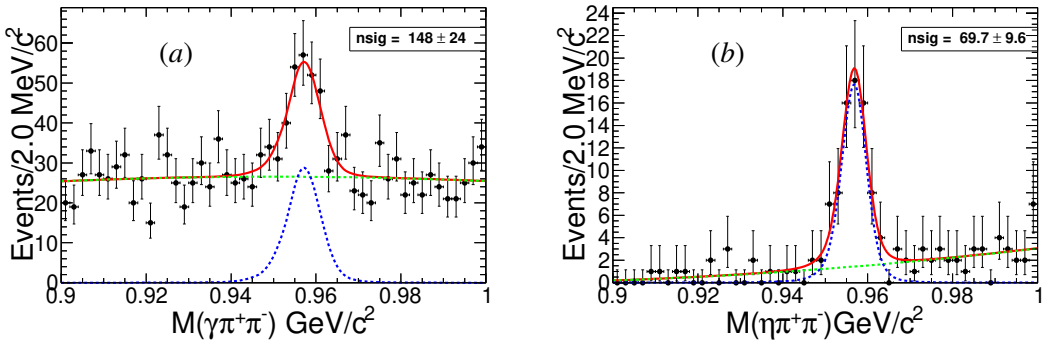

Figure 14: The fits to the mass spectra of M($\gamma\pi^+\pi^-$)(a) and M($\eta\pi^+\pi^-$)(b)

8 Systematic uncertainty

8.1 Number of $\psi(3686)$ events

Using the inclusive hadronic decays, the number of $\psi(3686)$ events is determined to be $22.6(1.0 \pm 0.63\%) \times 10^8$ [13]. By adding the number of $\psi(3686)$ events, $(448.1 \pm 2.9) \times 10^6$ [12], the number of $\psi(3686)$ events of the full data sample is calculated to be $(27.08 \pm 0.17) \times 10^8$, and the systematic uncertainty from this source is determined to be 0.7% .

8.2 Tracking efficiency

The uncertainty due to data-MC difference in the tracking efficiency is 1.0% for each charged track coming from a primary vertex according to a study of $J/\psi \to \rho\pi$ and $J/\psi \to p\bar{p}\pi^+\pi^-$ events [18]. For each track decays from $\Lambda/\bar{\Lambda}$, the uncertainty is also 1.0% from analysis of $J/\psi \to \bar{p}K^+\Lambda$ events [19]. In this analysis, the uncertainty from this source is assigned to be 6.0%.

8.3 PID efficiency

The PID efficiency have been investigated using control samples of $J/\psi \to p\bar{p}\pi^+\pi^-$. The uncertainty is assigned to be 1.0% per charged track. In this analysis, each charged tracks are applied PID , 6.0% uncertainty totally for this source .

8.4 Photon detection efficiency

The uncertainty in the photon reconstruction is studied by using the control sample $\psi(3686) \to \pi^+\pi^- J/\psi, J/\psi \to \rho^0\pi^0$ [20], and 1.0% systematic uncertainty is estimated for each photon.

8.5 Λ and $\bar{\Lambda}$ reconstruction efficiency

The uncertainties due to the Λ and $\bar{\Lambda}$ vertex fits are determined to be 1.0% each, which studied in $\psi(3686)/J/\psi \to \Lambda\bar{\Lambda}\eta(\pi^0)$ [2]. In this analysis, systematic uncertainty for one pair of $\Lambda\bar{\Lambda}$ is assigned to be 2.0%.

8.6 Kinematic fit

The systematic uncertainty due to kinematic fitting is estimated by correcting the helix parameters [21, 22] of charged tracks according the method described in Ref.[23]. The helix parameters are shown in Table. 6. In our analysis, we take the efficiency from the track-parameter-nocorrected MC samples as the nominal value, and take half of the difference between MC samples before and after the

correction as the systematic error from the kinematic fitting, which are both 0.55% both for **Mode I** and **Mode II**. The χ^2 comparisons with and without the correction are shown in Fig.15 .

8.7 Intermediate decays

The systematic uncertainties on the branching fractions of the intermediate-decays, including $\Lambda \to p\pi^-$, $\eta' \to \gamma\pi^+\pi^-$, $\eta' \to \pi^+\pi^-\eta$ and $\eta \to \gamma\gamma$, are quoted from PDG [3].

8.8 Mass window

The systematic uncertainties related to each mass window requirements are estimated by varying the size of the mass window . The maximum resulting differences of branching fractions are treated as the systematic uncertainties for each requirement.

8.9 Signal shape and background shape

To estimate the uncertainty due to the choice of signal shape, MC-simulated shape convolves Gauss function is replaced by MCshape and the resulting differences in the branching fraction is assigned as systematic uncertainty. As background shape , second order Chebychev function is replaced by third order polynomial . The difference of branching fraction is treated as uncertainty.

8.10 Fit range

The uncertainty of fitting range is estimated by varying fit range as (0.89,1.01)GeV/c^2, (0.89,0.99)GeV/c^2, (0.91,1.01)GeV/c^2 and (0.91,0.99)GeV/c^2, the maximum resulting difference is assigned to be uncertainty.

8.11 Summary of systematic uncertainty

The summaries of systematic uncertainties are listing on Table.7 and Table.8. Assuming all sources are independent, the total systematic uncertainty can be obtained by adding the individual contributions in quadrature.

Table 6: The correction parameters for p and π

	p	$\bar{p}$	π^+	π^-
ϕ_0	1.125	1.107	1.18	1.18
κ	1.168	1.112	1.21	1.21
$\tan\lambda$	1.090	1.062	1.13	1.12

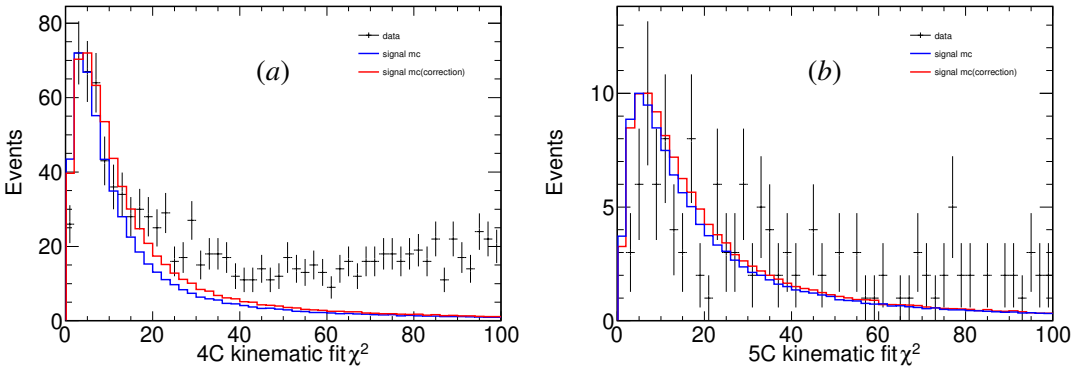

Figure 15: The χ^2 distribution for $\eta' \to \gamma\pi^+\pi^-$(a) and $\eta' \to \eta\pi^+\pi^-$(b)

.

Table 7: Systematic uncertainty for process $\eta' \to \gamma\pi^+\pi^-$

Source		Uncertainty(%)
$\psi(3686)$ total number*		0.7
MDC tracking*		6.0
PID efficiency*		6.0
Photon detection efficiency		1.0
Λ and $\bar{\Lambda}$ reconstruction efficiency*		2.0
Kinematic fit		0.55
Intermediate decays	$\Lambda \to p\pi^-$*	0.5
	$\bar{\Lambda} \to \bar{p}\pi^+$*	0.5
	$\eta' \to \gamma\pi^+\pi^-$	0.4
Mass window	$\Lambda(\pm 1 MeV/c^2)$	2.8
	$\bar{\Lambda}(\pm 1 MeV/c^2)$	1.9
	$J/\psi(\pm 2 MeV/c^2)$	0.8
	$\Sigma^0/\bar{\Sigma}^0(\pm 2 MeV/c^2)$	0.6
	$\chi_{c0}(\pm 3 MeV/c^2)$	1.5
	$\chi_{c1}(\pm 2 MeV/c^2)$	3.3
	$\chi_{c2}(\pm 2 MeV/c^2)$	3.8
	$\Xi^-/\bar{\Xi}^+(\pm 2 MeV/c^2)$	0.7
	$\Sigma(1385)(\pm 10 MeV/c^2)$	3.3
Fitting	Signal shape	0.7
	Background shape	2.0
	Fitting range	1.4
Total		11.7

Table 8: Systematic uncertainty for process $\eta' \to \eta\pi^+\pi^-$

Source		Uncertainty(%)
$\psi(3686)$ total number*		0.7
MDC tracking*		6.0
PID efficiency*		6.0
Photon detection efficiency		2.0
Λ and $\bar{\Lambda}$ reconstruction efficiency*		2.0
Kinematic fit		0.55
Intermediate decays	$\Lambda \to p\pi^-$*	0.5
	$\bar{\Lambda} \to \bar{p}\pi^+$*	0.5
	$\eta' \to \eta\pi^+\pi^-$	0.5
	$\eta \to \gamma\gamma$	0.18
Mass window	$\Lambda(\pm 1 MeV/c^2)$	1.7
	$\bar{\Lambda}(\pm 1 MeV/c^2)$	1.4
	$J/\psi(\pm 1 MeV/c^2)$	3.2
Fitting	Signal shape	0.7
	Background shape	1.2
	Fitting range	3.7
Total		10.6

8.12 Branching fraction result combination

The measured branching fractions from the two η' decay modes are consistent with each other within their uncertainties. The measurements from the two decay modes are, therefore, combined by considering the correlation of uncertainties between the two measurements, the mean value and the uncertainty are calculated with [24, 25]

$$\bar{x} \pm \sigma(\bar{x}) = \frac{\Sigma_j(x_j \cdot \Sigma_i w_{ij})}{\Sigma_i \Sigma_j w_{ij}} \pm \sqrt{\frac{1}{\Sigma_i \Sigma_j w_{ij}}} \tag{3}$$

where i and j are summed over all decay modes, w_{ij} is the element of the weight matrix $W = V_x^{-1}$, and V_x is the covariance error matrix calculated according to the statistical uncertainties and the systematic uncertainties. When combining the results of the two decay modes, the error matrix can be calculated as

$$V = \begin{pmatrix} \sigma_1^2 + \epsilon_f^2 x_1^2 & \epsilon_f^2 x_1 x_2 \\ \epsilon_f^2 x_1 x_2 & \sigma_2^2 + \epsilon_f^2 x_2^2 \end{pmatrix} \tag{4}$$

Where σ_i is the independent absolute uncertainty (the statistical uncertainty and all independent systematical uncertainties added in quadrature) in the measurement mode i, and ϵ_f is the common relative systematic uncertainties between the two measurements (All the common systematic uncertainties added in quadrature. The items in Table.7 and Table.8 with marked '*' are common uncertainties, and the other items are independent uncertainties). x_i is the measured value given by mode i. Then the combined mean

value and combined uncertainty can be calculated as :

$$\bar{x} = \frac{x_1\sigma_2^2 + x_2\sigma_1^2}{\sigma_1^2 + \sigma_2^2 + (x_1 - x_2)^2\epsilon_f^2} \tag{5}$$

$$\sigma(\bar{x}) = \sqrt{\frac{\sigma_1^2\sigma_2^2 + (x_1^2\sigma_2^2 + x_2^2\sigma_1^2)\epsilon_f^2}{\sigma_1^2 + \sigma_2^2 + (x_1 - x_2)^2\epsilon_f^2}} \tag{6}$$

The calculated results are shown in Table.9.

Table 9: Decay modes and branching fraction

Processes	Branching fraction
$\eta' \to \gamma\pi^+\pi^-$	$(6.97 \pm 1.13 \pm 0.82) \times 10^{-6}$
$\eta' \to \eta\pi^+\pi^-$	$(8.22 \pm 1.12 \pm 0.87) \times 10^{-6}$
Average	$(7.58 \pm 1.10) \times 10^{-6}$

9 Summary

Using the data sample of 2.7 billion $\psi(3686)$ events , the $\psi(3686) \to \Lambda\bar{\Lambda}\eta'$ decay is observed for the first time with the two decay modes of $\eta' \to \gamma\pi^+\pi^-$ (**Mode I**)and $\eta' \to \pi^+\pi^-\eta$ (**Mode II**) . The analysis results for **Mode I** and **Mode II** are summarized in Table.9, where the first uncertainties are statistical, and second ones are systematic. The average branching fraction of $\psi(3686) \to \Lambda\bar{\Lambda}\eta'$ is calculated to be $(7.58 \pm 1.10) \times 10^{-6}$, where the uncertainty includes both statistical and systematic. In case of excited states of $\Lambda^* \to \Lambda\eta'(\bar{\Lambda}^* \to \bar{\Lambda}\eta')$, there is no evident structure in mass distribution of $\Lambda\eta'$ or $\bar{\Lambda}\eta'$ bases on present statistics.

10 Appendix

The excited states of $\Lambda(\bar{\Lambda})$, consists of $\Lambda\eta'(\bar{\Lambda}\eta')$, the Dalitz plots and mass distribution shown in Fig.16.17.

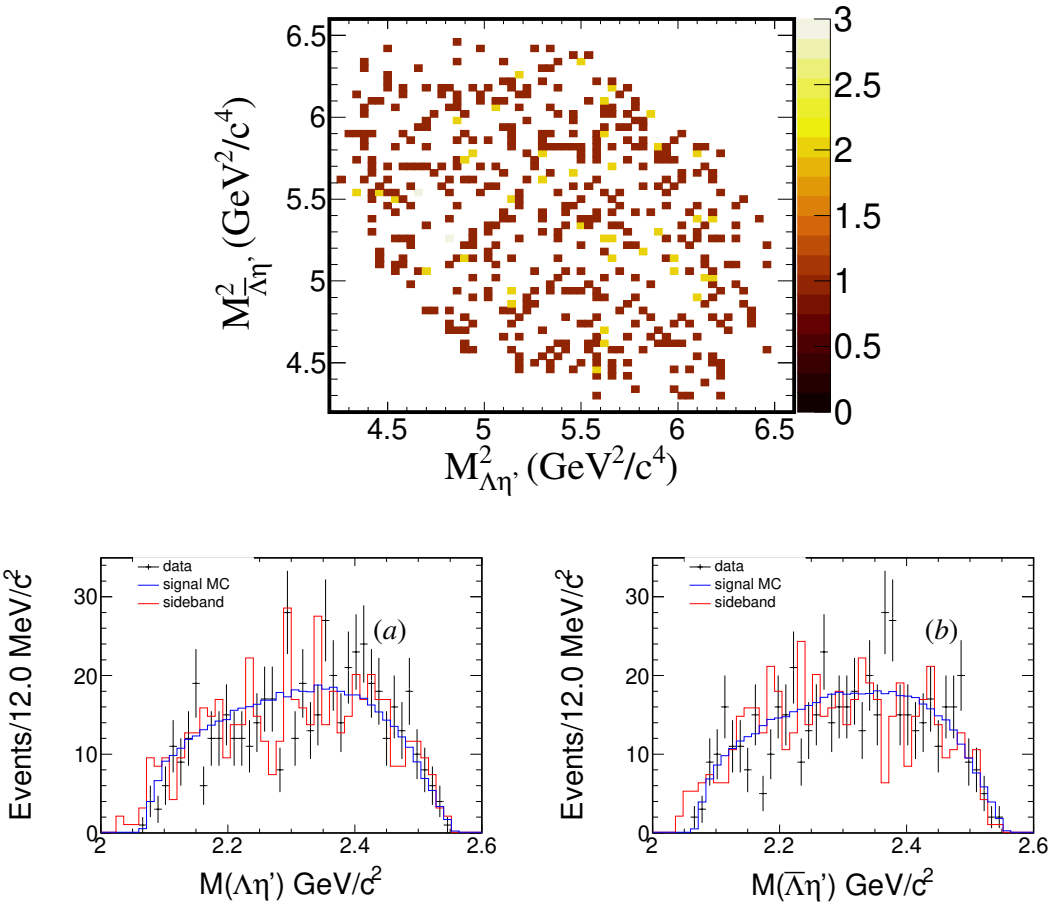

Figure 16: For Mode:$\eta' \to \gamma\pi^+\pi^-$, Dalitz plots of $M^2_{\Lambda\eta'}$ versus $M^2_{\bar{\Lambda}\eta'}$, and the mass distribution of $M_{\Lambda\eta'}$(a) and $M_{\bar{\Lambda}\eta'}$(b).

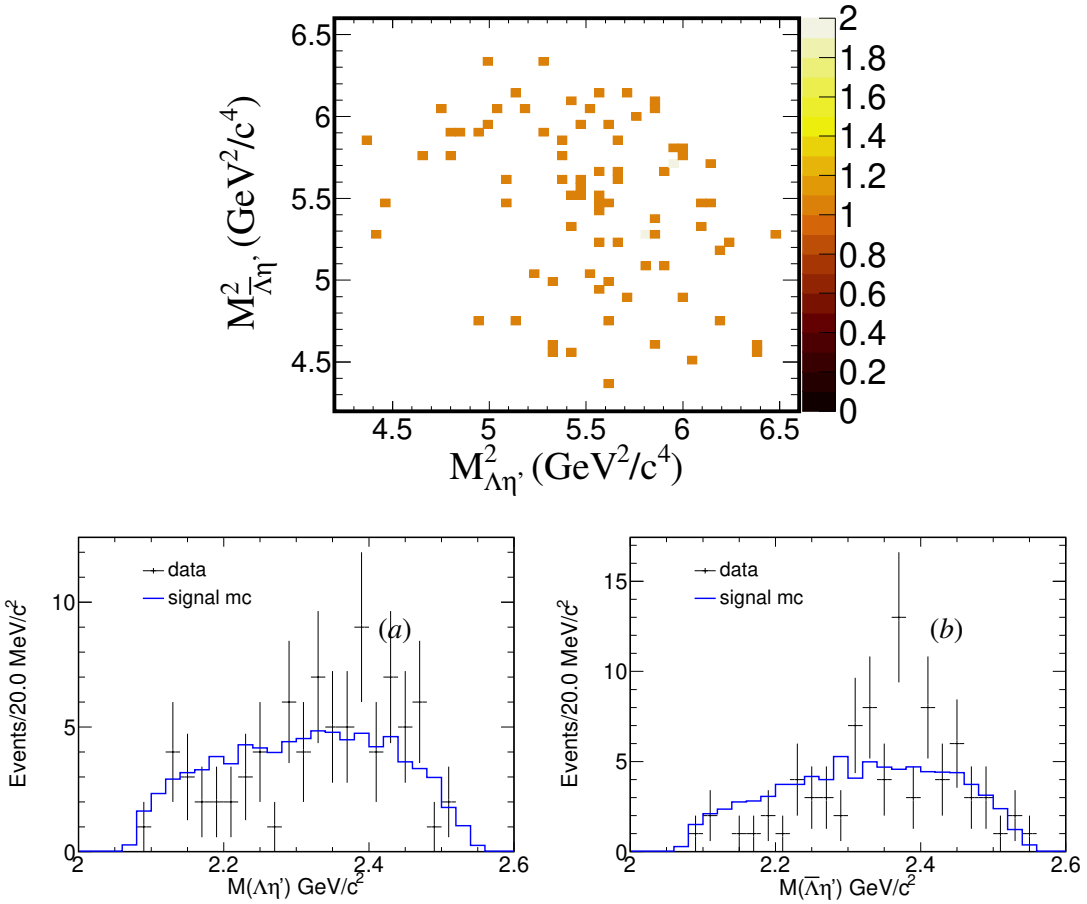

Figure 17: For Mode: $\eta' \to \eta\pi^+\pi^-$, Dalitz plots of $M^2_{\Lambda\eta'}$ versus $M^2_{\bar{\Lambda}\eta'}$, and the mass distribution of $M_{\Lambda\eta'}$(a) and $M_{\bar{\Lambda}\eta'}$(b).

References

[1] S. Wang, (2022), arXiv:2207.14350[hep-ex].

[2] M. Ablikim *et al.*[BESIII Collaboration], Phys. Rev.**D 87**, 052007 (2013)

[3] P. A. Zyla et al. [Particle Data Group], PTEP **2020**, 083C01 (2020).

[4] M. Ablikim *et al.*[BESIII Collaboration], Nucl. Instrum. Meth. **A 614**, 345 (2010).

[5] M. Ablikim *et al.*[BESIII Collaboration], Chin. Phys. **C 44**, 040001 (2020).

[6] S. Agostinelli *et al.*[GEANT4], Nucl. Instrum. Meth. **A 506**, 250 (2003).

[7] S. Jadach, and B. F. L. Ward and Z. Was, Phys. Rev. **D 63**, 113009 (2001).

[8] Comput. Phys. Commun. **130** 260(2000)

[9] D. J. Lange, Nucl. Instrum. Meth. **A 462**, 152 (2001).

[10] R. G. Ping, Chin. Phys. **C 32**, 599 (2008).

[11] J. C. Chen, G. S. Huang, X. R. Qi, D. H. Zhang and Y. S. Zhu, Phys. Rev. **D 62**, 034003 (2000).

[12] M. Ablikim *et al*. [BESIII Collaboration], Chin. Phys. **C 42**, 023001 (2018).

[13] Cheng. L (2022), https://indico.ihep.ac.cn/event/16632/contributions/49274/attachments/23536/26672/number_of_psi2S.pdf

[14] https://docbes3.ihep.ac.cn/~charmoniumgroup/index.php/Datasets#2022_3.65.2C_3.682_.28on-line.29

[15] M. Xu *et al.*, Chin. Phys. **C 33**, 428 (2009).

[16] X. Zhou, S. Du, G. Li, and C. Shen, Comput. Phys. Commun. **258**, 107540 (2021).

[17] M. Ablikim *et al.* [BESIII Collaboration], Chin. Phys. **C 36**, 915 (2012).

[18] M. Ablikim *et al.* [BESIII Collaboration], Phys. Rev. **D 85**, 092012 (2012).

[19] M. Ablikim *et al.* [BESIII Collaboration], Phys. Rev. **D 87**, 012007 (2013).

[20] M. Ablikim *et al.* [BESIII Collaboration], Phys. Rev. **D 83**, 112005 (2011).

[21] M. Ablikim *et al.* [BESIII Collaboration], Phys. Rev. **D 88**, 112001 (2013);

[22] https://docbes3.ihep.ac.cn/~charmoniumgroup/index.php/XYZProposal#The_helix_correction_factors

[23] M. Ablikim *et al.* [BESIII Collaboration], Phys. Rev. **D 87**, 012002 (2013)

[24] Z.T . Sun, (2014), arXiv:1402.2023 [hep-ex].

[25] M. Ablikim *et al.* [BESIII Collaboration], Phys. Rev. **D 89**, 074030 (2004).